



Cite this: *Phys. Chem. Chem. Phys.*, 2016, **18**, 12074

Flexible additive free $\text{H}_2\text{V}_3\text{O}_8$ nanowire membrane as cathode for sodium ion batteries†

Di Wang,‡ Qiulong Wei,‡ Jinzhi Sheng, Ping Hu, Mengyu Yan, Ruimin Sun, Xiaoming Xu, Qinyou An* and Liqiang Mai*

Sodium ion batteries (SIBs) have emerged as a potential candidate to succeed lithium ion batteries (LIBs), because of the abundant sodium resources on earth. Layered vanadium oxides are regarded as the promising candidates for SIBs because of their large interlayer spacing, high theoretical specific capacity, abundant sources and low cost. In this paper, a vanadium oxide hydrate ($\text{H}_2\text{V}_3\text{O}_8$) nanowire membrane is presented as a flexible cathode for SIBs without addition of any other additives (binders or conductive compounds). Such a freestanding flexible membrane exhibits a high specific capacity of 168 mA h g^{-1} at 10 mA g^{-1} , and its high capacity is maintained well after 100 cycles. It is found that the capacitive charge storage accounts for a relatively large proportion of the total capacity, whereas the crystal structure of $\text{H}_2\text{V}_3\text{O}_8$ is highly reversible during the sodiation/desodiation processes. This research demonstrates that the $\text{H}_2\text{V}_3\text{O}_8$ nanowire is an exceptional candidate for SIBs.

Received 2nd February 2016,
Accepted 26th March 2016

DOI: 10.1039/c6cp00745g

www.rsc.org/pccp

Introduction

With the rapid development of clean renewable energy and increasing demands for electronic devices, electric vehicles and energy grid, tremendous efforts have been made to exploit large-scale energy storage devices with high performances and low cost.^{1–4} Over the past decades, lithium ion batteries (LIBs) have become the most promising rechargeable batteries and are widely used commercially, because of their high energy density and long cycle life.^{5–10} Nevertheless, because of the limited lithium resources and increased prices, the further development of LIBs is hindered.¹¹ Therefore, a substitute with abundant resources and low cost is highly desirable. Sodium ion batteries (SIBs) are, therefore, an ideal substitute for LIBs, because of the abundant resources of sodium and their similar electrochemical mechanism to LIBs.^{12–15} However, the radius of sodium (0.97 \AA) is 1.43 times the size of lithium (0.68 \AA). The large size of sodium leads to severe structure degradation and sluggish diffusion kinetics during the intercalation/deintercalation process.^{16–18} Thus, it is urgent to

exploit new electrode materials with a large open structure for sodium ion storage.

Layered vanadium oxides have been developed recently and are regarded as promising candidates for SIBs because of their large interlayer spacing, high theoretical specific capacity, abundant sources and low cost.^{19–24} Among the family of layered vanadium oxides, vanadium oxide hydrate ($\text{H}_2\text{V}_3\text{O}_8$), formed by V_3O_8 layers comprised of VO_6 octahedrons and VO_5 trigonal bipyramids, has a large interlayer spacing, which is beneficial for sodium storage.²⁵ Also, hydrogen atoms are linked with VO_6 octahedrons and the octahedrons in the next layer to form hydrogen bonds, which hold the V_3O_8 layers.²⁶ Compared with typical vanadium pentoxide (V_2O_5), in which van der Waals bonds hold the layers together, $\text{H}_2\text{V}_3\text{O}_8$ with hydrogen bonds provides an elastic buffer space for volume expansion/contraction during cycling.^{27–31} Furthermore, $\text{H}_2\text{V}_3\text{O}_8$ contains mixed valences of V^{5+} and V^{4+} , which contribute to higher electronic conductivity and more active redox sites during the charging and discharging process.^{32,33} The unique structure indicates that $\text{H}_2\text{V}_3\text{O}_8$ is a promising material for sodium storage. However, its sodium storage performance and detailed mechanism have been rarely reported.

Besides the active materials, a whole electrode mainly contains the polymeric binders, conductive additives and current collectors in a conventional battery system. The polymeric binders and conductive materials are used to mechanically secure the materials and provide an electrical contact between the active materials and current collectors. However, the existence of polymeric binders decreases the electrical conductivity, which hinders the ion transfer in the active materials and

State Key Laboratory of Advanced Technology for Materials Synthesis and Processing, Wuhan University of Technology, Wuhan, 430070, P. R. China.
E-mail: mlq518@whut.edu.cn, anqinyou86@whut.edu.cn

† Electronic supplementary information (ESI) available: The optical photograph and SEM images of the $\text{H}_2\text{V}_3\text{O}_8$ nanowire membrane after 100 cycles; the Nyquist plots of the $\text{H}_2\text{V}_3\text{O}_8$ nanowire membrane before cycling and after 100 cycles; EDX element mapping, SAED pattern, TEM images of the $\text{H}_2\text{V}_3\text{O}_8$ nanowire membrane discharged to 1.5 V; high-resolution XPS spectrum of Na 1s of the $\text{H}_2\text{V}_3\text{O}_8$ nanowire membrane discharged to 1.5 V. See DOI: 10.1039/c6cp00745g

‡ These authors contributed equally to this work.

increases the polarization of the electrodes.^{34,35} Furthermore, the polymeric binders and conductive materials occupy about 20–40% of the total electrode mass, which do not deliver actual capacity.^{36,37} Meanwhile, these foreign components also obstruct the characterization and investigation of the relationship between electrochemical performance and structure of active materials. Active materials may easily fall off the conductive metal foils and it is difficult to maintain the original shape of the metallic current collectors after destruction. Alternatively, flexible freestanding films may reach a higher capacity and have better cycling stability than the conventional electrodes.^{38,39} Recently, Ghidui *et al.* reported an additive free, two-dimensional titanium carbide film,⁴⁰ exhibiting a volumetric capacitance up to 900 F cm^{-3} , with excellent cycling stability and rate capability. Zhang *et al.* fabricated a free standing defect rich molybdenum disulfide/graphene/carbon nanotube hybrid paper,⁴¹ which can be directly used as a flexible binder free anode for LIBs with a high reversible capacity of $1137.2 \text{ mA h g}^{-1}$ at the current density of 0.1 A g^{-1} . The nanowires, in particular, have been proved to be able to directly form the flexible film as a flexible electrode.^{42,43} Inspired by the previous reports, a flexible additive free film constructed by ultralong nanowires has a stable structure and high specific capacity, and provides pure testing environments without any other influence from foreign materials, which can be used to gain an insight into the relationship between the electrochemical performance and structure of the active materials.

In this paper, a flexible, additive free $\text{H}_2\text{V}_3\text{O}_8$ nanowire membrane synthesized *via* a simple hydrothermal method followed by a suction filtration process is presented. The $\text{H}_2\text{V}_3\text{O}_8$ membrane is investigated as the cathode for SIBs, and exhibits an excellent sodium storage ability with a high specific capacity of 168 mA h g^{-1} at a current density of 10 mA g^{-1} , as well as an amazing cycling stability during charge and discharge processes. The sodium ion storage mechanism of the $\text{H}_2\text{V}_3\text{O}_8$ nanowire membrane is also studied further. The results indicate that the capacitive charge storage accounts for a relatively large proportion of the total capacity, the crystal structure of $\text{H}_2\text{V}_3\text{O}_8$ and the morphology of nanowire membrane display excellent structure stability during charge and discharge processes.

Experimental

Synthesis of $\text{H}_2\text{V}_3\text{O}_8$ nanowires

The $\text{H}_2\text{V}_3\text{O}_8$ nanowires were prepared by a simple, modified one-step hydrothermal method.^{22,27} The $\text{H}_2\text{V}_3\text{O}_8$ nanowires were obtained in two steps. First, $1.3 \text{ mmol V}_2\text{O}_5$ powder (0.237 g), 50 ml deionized water and 0.04 g poly(ethylene glycol) (PEG-4000) were successively added into 10 mL 30% hydrogen peroxide under vigorous stirring, and the as-obtained orange solution was stirred continuously for one day at ambient conditions. Then the mixed solution was sealed into a 100 mL Teflon lined stainless steel autoclave and hydrothermally treated at $180 \text{ }^\circ\text{C}$ for 60 h . The products were collected and washed with deionized water and ethanol repeatedly to obtain the pure ultralong $\text{H}_2\text{V}_3\text{O}_8$ nanowires.

Fabrication of the flexible additive free $\text{H}_2\text{V}_3\text{O}_8$ nanowire membrane

The flexible additive free $\text{H}_2\text{V}_3\text{O}_8$ nanowire membrane was fabricated using a suction filtration process. In the typical procedure, a designated amount of $\text{H}_2\text{V}_3\text{O}_8$ nanowires were treated by an ultrasound process for 1 h . Subsequently, the suspension was filtrated through a poly(vinylidene fluoride) membrane filter (220 nm pore size, Durapore[®] from Sigma-Aldrich). After peeling off the membrane from the membrane filter, the as-fabricated $\text{H}_2\text{V}_3\text{O}_8$ membrane was placed in ambient conditions for several hours to evaporate the water absorbed in it, and then dried at $80 \text{ }^\circ\text{C}$ for 12 h in air.

Materials characterization

X-ray diffraction (XRD) measurements were performed to investigate the crystallographic information using a Bruker D8 Advance X-ray diffractometer with a non-monochromated $\text{Cu K}\alpha$ X-ray source. Scanning electron microscopy (SEM) images were collected with a Jeol JSM-7100F field emission scanning electron microscope at an acceleration voltage of 15 kV . Transmission electron microscopy (TEM) and high resolution transmission electron microscopy (HRTEM) images were recorded with a Jeol JEM-2100F scanning transmission electron microscope/energy dispersive X-ray spectroscopy (EDX) microscope. Fourier transform – infrared (FTIR) transmittance spectra were recorded using a Nicolet 60-SXB IR spectrometer. X-ray photoelectron spectroscopy (XPS) measurements were performed using a VG MultiLab 2000 instrument.

Electrochemical measurements

The electrochemical properties were measured using CR2016 coin cells assembled in a glove box filled with pure argon gas. For the preparation of the electrodes, the $\text{H}_2\text{V}_3\text{O}_8$ membrane was cut into pieces with an area of about 0.5 cm^2 and a loading of $\sim 1.5 \text{ mg cm}^{-2}$. For the fabrication of the sodium batteries, sodium metal was used as the anode, a 1 M solution of sodium perchlorate in ethylene carbonate/propylene carbonate with a volume ratio of $1 : 2$ was used as the electrolyte, and a Whatman Glass microfibre filter (Grade GF/F) was used as the separator. Before the charging/discharging process, the cells were aged for several hours to ensure full absorption of the electrolyte. Galvanostatic charging/discharging tests were performed in the voltage range of 1.5 to 4 V versus Na^+/Na at different current densities on a multichannel battery testing system (LANDT CT2001A). Cyclic voltammetry (CV) curves and electrochemical impedance spectroscopy were recorded using electrochemical workstations (Autolab PGSTAT302N and CHI 760D). All the tests were performed at room temperature.

Results and discussion

The illustration of the fabrication processes for a flexible additive free $\text{H}_2\text{V}_3\text{O}_8$ nanowire membrane is shown in Fig. 1a. The $\text{H}_2\text{V}_3\text{O}_8$ nanowire membrane was obtained *via* a hydrothermal reaction and suction filtration process. The as-obtained membrane

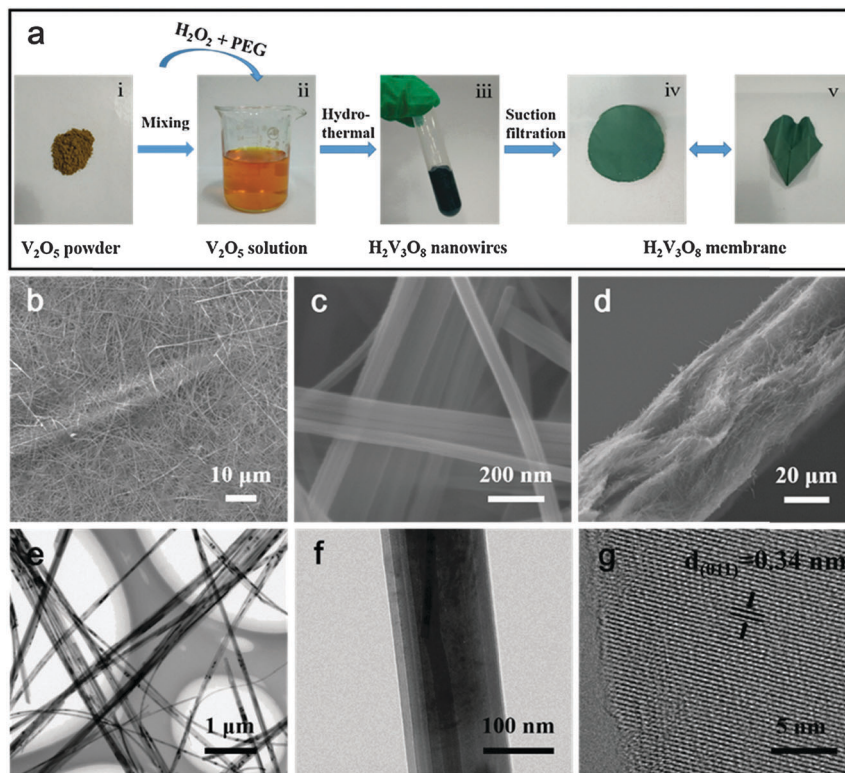


Fig. 1 (a) A schematic illustration for the formation of the flexible additive free $\text{H}_2\text{V}_3\text{O}_8$ nanowire membrane using a hydrothermal reaction followed by a suction filtration method. Front (b and c) and side (d) SEM images of the $\text{H}_2\text{V}_3\text{O}_8$ nanowire membrane. TEM (e and f) and HRTEM (g) images of the $\text{H}_2\text{V}_3\text{O}_8$ nanowire membrane.

can be folded into a paper airplane and can be well recovered after spreading (Fig. 1a), which demonstrates the excellent flexibility of the membrane. SEM and TEM images (Fig. 1b–f) show that the membrane is composed of uniform $\text{H}_2\text{V}_3\text{O}_8$ nanowires of ~ 100 nm in width and hundreds of micrometers in length. The assembled membrane is ~ 35 μm in thickness (Fig. 1d). The HRTEM image (Fig. 1g) shows the lattice fringes of the as-synthesized nanowire possessing a d -spacing of 0.34 nm, which matches well with the (011) plane of $\text{H}_2\text{V}_3\text{O}_8$. The ultralong $\text{H}_2\text{V}_3\text{O}_8$ nanowires are the key advantage for the fabrication of highly flexible membranes. For the synthesis of an ultralong nanowire, the long chain linear polymer molecule PEG was used as a template and reductant during the hydrothermal reaction.²⁷

To investigate the crystallographic structure of the $\text{H}_2\text{V}_3\text{O}_8$ nanowire membrane, the XRD pattern was obtained (Fig. 2a). All peaks of the membrane are consistent with orthorhombic $\text{H}_2\text{V}_3\text{O}_8$ (JCPDS No. 01-085-2401) with a $Pnam$ space group and lattice parameters of $a = 16.9298$ \AA , $b = 9.3598$ \AA , $c = 3.6443$ \AA , $\alpha = \beta = \gamma = 90^\circ$. Meanwhile, the sharp diffraction peaks demonstrate good crystallinity of the obtained $\text{H}_2\text{V}_3\text{O}_8$ nanowires. To further confirm the bonds in the $\text{H}_2\text{V}_3\text{O}_8$ structure, the FTIR spectrum was measured (Fig. 2b). The peak located at 564 cm^{-1} comes from the stretching vibrations of the V–O–V bridging bonds. The strong absorption bands at 974 and 1022 cm^{-1} are attributed to the symmetric stretching of $\text{V}^{4+}=\text{O}$ and $\text{V}^{5+}=\text{O}$ bonds, respectively. The bands at 1630 and 3424 cm^{-1}

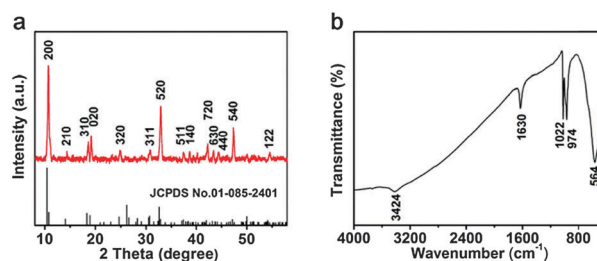


Fig. 2 (a) XRD pattern and (b) FTIR spectrum of the $\text{H}_2\text{V}_3\text{O}_8$ nanowire membrane.

correspond to the vibrations of water molecules and O–H bands, respectively.^{30,44} The results indicate that the material consists of mixed valence states of vanadium atoms and O–H bands.

The electrochemical performances of the $\text{H}_2\text{V}_3\text{O}_8$ nanowire membrane were characterized by using CR2016 coin cells with sodium metal as the counter electrode. The CV curve of the $\text{H}_2\text{V}_3\text{O}_8$ membrane was measured at a scan rate of 0.1 mV s^{-1} with the potential range of 1.5 – 4 V versus Na^+/Na at room temperature (Fig. 3a). The cathodic and anodic peaks were ascribed to the sodium ion insertion and extraction in the cathode, respectively. Two cathodic peaks were situated at the potentials of 2.9 and 3.1 V, whereas the two anodic peaks were observed at 3.1 and 3.3 V. The electrochemical performance was further evaluated using galvanostatic discharge/charge testing.

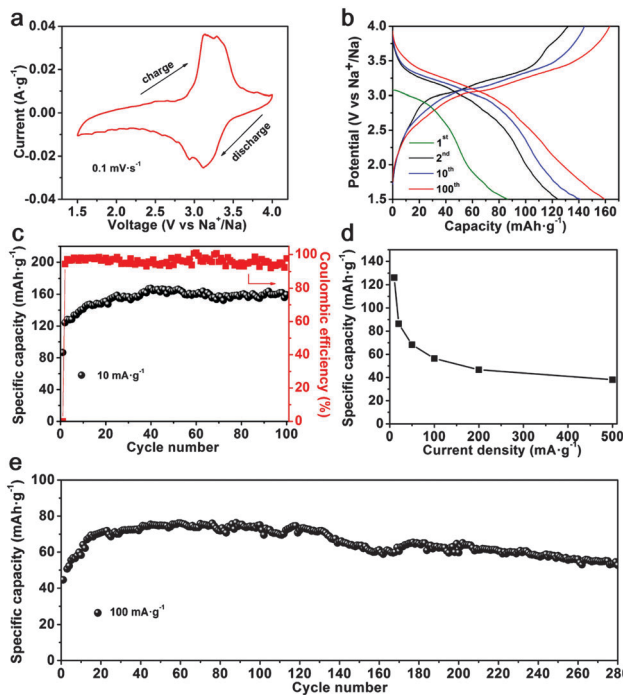


Fig. 3 (a) CV curve of the $\text{H}_2\text{V}_3\text{O}_8$ nanowire membrane at a scan rate of 0.1 mV s^{-1} . (b) Discharge-charge curves of the $\text{H}_2\text{V}_3\text{O}_8$ nanowire membrane at different cycles under 10 mA g^{-1} . (c) Cycling performance of the $\text{H}_2\text{V}_3\text{O}_8$ membrane at the current density of 10 mA g^{-1} . (d) Rate performance of the $\text{H}_2\text{V}_3\text{O}_8$ membrane. (e) Cycling performance at the current density of 100 mA g^{-1} .

Fig. 3b displays the charge-discharge voltage profile of the $\text{H}_2\text{V}_3\text{O}_8$ membrane at the current density of 10 mA g^{-1} . There are two pairs of slight plateaus which correspond well with the CV results. Fig. 3c shows the cycling performance of the $\text{H}_2\text{V}_3\text{O}_8$ membrane at the current density of 10 mA g^{-1} . The first discharge capacity is 87 mA h g^{-1} , which is lower than that of the following cycles, this may be because of the gradual diffusion of the electrolyte during the initial cycles, facilitating the electrochemical reaction and leading to the increase of capacity in the subsequent cycles. A similar phenomenon has been observed previously.²⁰ The second discharge capacity is 124 mA h g^{-1} , and the discharge capacity gradually increases to 168 mA h g^{-1} [about 1.8 sodium ions insertion per unit formula (eqn (S1), ESI†)] in the following 40 cycles. After 100 cycles, the discharge capacity is

maintained at 160 mA h g^{-1} , and the morphologies of the membrane and $\text{H}_2\text{V}_3\text{O}_8$ nanowires remain undestroyed (Fig. S1, ESI†). The results discussed above demonstrate the excellent reversibility of the $\text{H}_2\text{V}_3\text{O}_8$ nanowire membrane during the charge-discharge processes. The Nyquist plots in Fig. S2 (ESI†) show that the charge transfer resistance of the cell decreases from $4700 \text{ }\Omega$ after 100 cycles, which is 0.42 times of the initial state. This is possibly because the electrolyte gradually penetrates into the material and the material becomes more active along with the cycling, which accounts for the increase of capacity during the initial 40 cycles as well.⁴⁵ For further evaluation of the electrochemical behaviour, the rate capability of the $\text{H}_2\text{V}_3\text{O}_8$ membrane was measured at various current densities ranging from 10 to 500 mA g^{-1} (Fig. 3d). The membrane delivers the discharge capacity of 125, 86, 68, 56, 46 and 38 mA h g^{-1} at the current density of 10, 20, 50, 100, 200 and 500 mA g^{-1} , respectively. The cycling performance at the current density of 100 mA g^{-1} is displayed in Fig. 3e. The initial specific discharge capacity is 45 mA h g^{-1} . The capacity increases to 76 mA h g^{-1} after 60 cycles, and after 280 cycles, the capacity is still maintained at 53 mA h g^{-1} . The flexible membrane contains only $\text{H}_2\text{V}_3\text{O}_8$ nanowires without any other binders or conductive additives. The excellent performances are obtained just from the additive free membrane, which has never been achieved before.

CV curves at different scan rates were measured to evaluate the electrochemical kinetics of electrode materials in SIBs. It is known that the total capacity is controlled by two different charge-storage mechanisms: the diffusion-controlled Faradaic reaction and the capacity behaviour (non-Faradaic electrical double layer capacitance and pseudocapacitance).^{24,46} Fig. 4a shows the CV curves at different scan rates from 0.05 to 0.5 mV s^{-1} . With the increases of the scan rate, the cathodic and anodic peaks slightly shift to lower and higher potentials, respectively. The total capacity at a certain scan rate could be quantified by separating the specific contribution to diffusion controlled capacity and capacitance with the analysis proposed by Dunn and coworkers.⁴⁷ The total current response (i) at a fixed potential (V) can be regarded as the combination of the two mechanisms (eqn (1)):

$$i(V) = k_1v + k_2v^{1/2} \quad (1)$$

where k_1v represents the total capacitive contribution and $k_2v^{1/2}$ stands for the contribution of the diffusion controlled Faradic intercalation process.⁴⁶ Fig. 4b gives the observation to

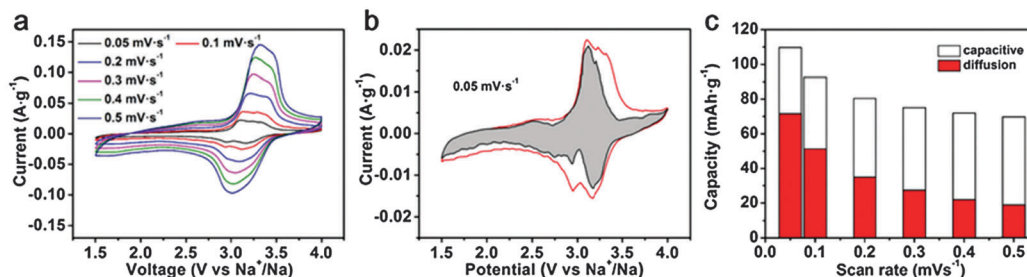


Fig. 4 (a) CV curves of the $\text{H}_2\text{V}_3\text{O}_8$ nanowire membrane at different scan rates. (b) Separation of capacitive and diffusion controlled charge storage at a scan rate of 0.05 mV s^{-1} . (c) Capacity contributions at different scan rates.

the capacity contributions at the scan rate of 0.05 mV s^{-1} , in which the shaded area corresponds to the diffusion controlled current response. The diffusion controlled charge is mainly generated at around the peak voltages, indicating that the diffusion processes at these regions are related to the redox reactions. Based on the calculation, the diffusion controlled charge occupied 64% of the total charge. Contribution ratios of the two different processes at other scan rates were also calculated (Fig. 4c). With the scan rate increases to 0.5 mV s^{-1} , the contribution of the diffusion controlled charge storage decreases to 26%. These results show that the capacitive charge storage contributes to a relatively large proportion of the total capacity.

Ex situ XRD, FTIR and XPS measurements were carried out to investigate the sodium storage mechanisms of the $\text{H}_2\text{V}_3\text{O}_8$ nanowire membrane at different charge and discharge states. Fig. 5a and Fig. S3a (ESI[†]) show the XRD patterns of the $\text{H}_2\text{V}_3\text{O}_8$ membrane at different states and after 280 cycles, respectively. The main diffractions exhibit little change even after long-term cycles, suggesting that there is a stable layered structure of $\text{H}_2\text{V}_3\text{O}_8$ during the sodiation/de-sodiation processes. From the magnified patterns of the (200) diffraction (inset in Fig. 5a), slightly reversible shifts were observed during discharge–charge processes. When first discharged to 1.5 V, the peak shifts to a higher degree, reflecting a small decrease of interlayer spacing, which may result from the intercalation of sodium ions that enhances the coordination reaction with the stacked layers and makes the interlayer spacing contract slightly. A similar phenomenon was also observed in the $\text{V}_2\text{O}_5 \cdot n\text{H}_2\text{O}$ after ion intercalation.^{24,48} When the voltage returns back to 4 V, the (200) diffraction gradually shifts back to its original degree. Other diffractions show slight shifts during the charge and discharge processes, which accompany the distortion of crystal structure. FTIR spectra of the cathode were measured to further investigate the structural changes (Fig. 5b and Fig. S3b, ESI[†]). The peak at 564 cm^{-1} (V–O–V vibrations) almost remains

unchanged during cycling, indicating the stability of the V–O structure. Before discharging, the peaks at 1022 and 974 cm^{-1} are sharp and separated. After discharging to 1.5 V, the peaks become broad and red shift, indicating the reduction of vanadium. These two peaks could almost be recovered after re-charging to 4.0 V, demonstrating a highly reversible faradic redox reaction during sodiation/desodiation. Furthermore, the vibrations of O–H bands (1630 and 3424 cm^{-1}) still exist after 280 cycles (Fig. S3b, ESI[†]), confirming the stable structure of V_3O_8 layers in which the O–H bonds are not totally exchanged during sodiation and desodiation.

XPS spectra were measured to detect the valence states of the cathode at two states: initial and discharged to 1.5 V. The survey spectra (Fig. 5c) reveal that all the samples consist of V and O, where the C is for calibration. High resolution spectra were also recorded to help understand the valence states of V (Fig. 5d). The spectrum observed from the sample at the initial state shows two main peaks. The V $2p_{3/2}$ peak is composed of two different peaks located at 516.3 and 517.5 eV, corresponding to V^{4+} and V^{5+} , respectively. Similarly, V $2p_{1/2}$ is composed of two different peaks located at 523.4 and 524.6 eV, corresponding to V^{4+} and V^{5+} , respectively.²⁸ After discharging to 1.5 V, the peaks of V^{5+} weaken and the peaks of V^{4+} strengthen, indicating that parts of V^{5+} are reduced to V^{4+} when sodium ions insert into the cathode (Fig. S4 and S5, ESI[†]).

Conclusions

A flexible $\text{H}_2\text{V}_3\text{O}_8$ nanowire membrane was successfully synthesized *via* a simple hydrothermal method followed by a suction filtration process. Such a freestanding membrane is constructed only from ultralong $\text{H}_2\text{V}_3\text{O}_8$ nanowires and exhibits remarkable flexibility. Applied as a cathode for SIBs, without addition of any other binders and conductive additives, the flexible, additive free $\text{H}_2\text{V}_3\text{O}_8$ nanowire membrane exhibits a high specific capacity of 168 mA h g^{-1} at 10 mA g^{-1} , and almost no capacity loss, no damage of the $\text{H}_2\text{V}_3\text{O}_8$ nanowires and membrane after 100 cycles. According to CV, *ex situ* XRD, FTIR and XPS analyses, it is found that layered $\text{H}_2\text{V}_3\text{O}_8$ stores sodium ions with a slight structural breathing effect. The capacitive charge storage accounts for a relatively large proportion of the total capacity. These results demonstrate that $\text{H}_2\text{V}_3\text{O}_8$ with a large interlayer spacing is a promising candidate material for sodium-based energy storage. The studies on the synthesis and performances of the flexible additive free $\text{H}_2\text{V}_3\text{O}_8$ nanowire membrane lay the foundation for further exploration of vanadium oxides for SIBs and the development of flexible devices.

Acknowledgements

This work was supported by the National Basic Research Program of China (2013CB934103, 2012CB933003), the International Science and Technology Cooperation Program of China (2013DFA50840), the National Natural Science Foundation of China (51521001, 51272197, 51302203), the National Natural

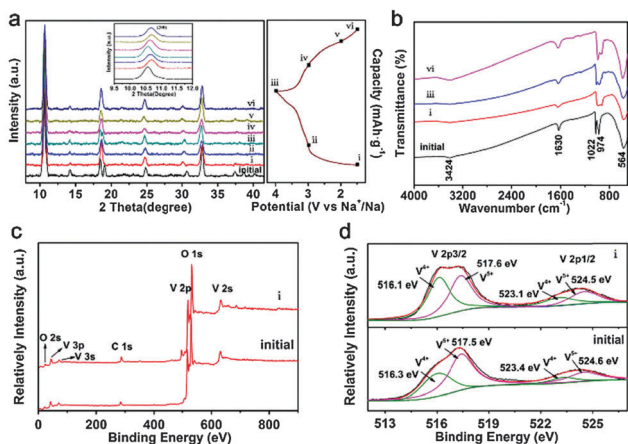


Fig. 5 *Ex situ* XRD patterns and the magnified patterns of (200) diffraction (inset) (a), FTIR spectra (b) and XPS spectra (c and d) of the $\text{H}_2\text{V}_3\text{O}_8$ nanowire membrane at various states: initial state, (i) discharge to 1.5 V, (ii) charge to 3 V, (iii) charge to 4 V, (iv) discharge to 3 V, (v) discharge to 2 V, (vi) discharge to 1.5 V.

Science Fund for Distinguished Young Scholars (51425204), the Hubei Province Natural Science Fund for Distinguished Young Scholars (2014CFA035), the Fundamental Research Funds for the Central Universities (WUT: 2015-III-021, 2015-III-032, 2015-III-052, 2015-PY-2), and the Students Innovation and Entrepreneurship Training Program (20151049701019).

Notes and references

- S. Chu and A. Majumdar, *Nature*, 2012, **488**, 294.
- L. Mai, X. Tian, X. Xu, L. Chang and L. Xu, *Chem. Rev.*, 2014, **114**, 11828.
- F. Cheng, J. Liang, Z. Tao and J. Chen, *Adv. Mater.*, 2011, **23**, 1695.
- L. Zhang, K. Zhao, W. Xu, Y. Dong, R. Xia, F. Liu, L. He, Q. Wei, M. Yan and L. Mai, *Phys. Chem. Chem. Phys.*, 2015, **17**, 7619.
- T. H. Kim, J. S. Park, S. K. Chang, S. Choi, J. H. Ryu and H. K. Song, *Adv. Energy Mater.*, 2012, **2**, 860.
- M. Armand and J. M. Tarascon, *Nature*, 2008, **451**, 652.
- J. B. Goodenough and K. S. Park, *J. Am. Chem. Soc.*, 2013, **135**, 1167.
- L. Zhang, J. Ni, W. Wang, J. Guo and L. Li, *J. Mater. Chem. A*, 2015, **3**, 11782.
- Z. Jian, W. Luo and X. Ji, *J. Am. Chem. Soc.*, 2015, **137**, 11566.
- S. Liang, J. Zhou, G. Fang, C. Zhang, J. Wu, Y. Tang and A. Pan, *Electrochim. Acta*, 2014, **130**, 119.
- D. Larcher and J. Tarascon, *Nat. Chem.*, 2015, **7**, 19.
- K. Zhang, Z. Hu, X. Liu, Z. L. Tao and J. Chen, *Adv. Mater.*, 2015, **27**, 3305.
- C. Zhu, P. Kopold, W. Li, P. A. Aken, J. Maier and Y. Yu, *J. Mater. Chem. A*, 2015, **3**, 20487.
- C. Wu, P. Kopold, Y. L. Ding, P. A. Aken, J. Maier and Y. Yu, *ACS Nano*, 2015, **9**, 6610.
- K. Zhang, Z. Hu, X. Liu, Z. Tao and J. Chen, *Adv. Mater.*, 2015, **27**, 3305.
- H. Pan, Y. Hu and L. Chen, *Energy Environ. Sci.*, 2013, **6**, 2338.
- V. Raju, J. Rains, C. Gates, W. Luo, X. Wang, W. F. Stickle, G. D. Stucky and X. Ji, *Nano Lett.*, 2014, **14**, 4119.
- N. Yabuuchi, K. Kubota, M. Dahbi and S. Komaba, *Chem. Rev.*, 2014, **114**, 11636.
- V. Raju, J. Rains, C. Gates, W. Luo, X. Wang, W. F. Stickle, G. D. Stucky and X. Ji, *Nano Lett.*, 2014, **14**, 4119.
- D. Su and G. Wang, *ACS Nano*, 2013, **7**, 11218.
- D. Hamani, M. Ati, J. M. Tarascon and P. Rozier, *Electrochem. Commun.*, 2011, **13**, 938.
- Y. Dong, S. Li, K. Zhao, C. Han, W. Chen, B. Wang, L. Wang, B. Xu, Q. Wei, L. Zhang, X. Xu and L. Mai, *Energy Environ. Sci.*, 2015, **8**, 1267.
- H. He, G. Jin, H. Wang, X. Huang, Z. Chen, D. Sun and Y. Tang, *J. Mater. Chem. A*, 2014, **2**, 3563.
- Q. Wei, J. Liu, W. Feng, J. Sheng, X. Tian, L. He, Q. An and L. Mai, *J. Mater. Chem. A*, 2015, **3**, 8070.
- V. Legagneur, A. L. G. La Salle, A. Verbaere, Y. Piffard and D. Guyomard, *J. Mater. Chem.*, 2000, **10**, 2805.
- Y. Mettan, R. Caputo and T. Chatterji, *RSC Adv.*, 2015, **5**(129), 106543.
- Q. An, J. Sheng, X. Xu, Q. Wei, Y. Zhu, C. Han, C. Niu and L. Mai, *New J. Chem.*, 2014, **38**, 2075.
- H. Li, T. Zhai, P. He, Y. Wang, E. Hosono and H. Zhou, *J. Mater. Chem.*, 2011, **21**, 1780.
- Y. Zhang, X. Liu, G. Xie, L. Yu, S. Yi, M. Hu and C. Huang, *Mater. Sci. Eng., B*, 2010, **175**, 164.
- V. Legagneur, A. L. G. La Salle, A. Verbaere, Y. Piffard and D. Guyomard, *Electrochim. Acta*, 2002, **47**, 1153.
- M. Yan, F. Wang, C. Han, X. Ma, X. Xu, Q. An, L. Xu, C. Niu, Y. Zhao, X. Tian, P. Hu, H. Wu and L. Mai, *J. Am. Chem. Soc.*, 2013, **135**, 18176.
- J. Xu, H. Sun, Z. Li, S. Lu, X. Zhang, S. Jiang, Q. Zhu and G. S. Zakhharova, *J. Solid State Ionics*, 2014, **262**, R72.
- C. Zhang, H. Song, C. Liu, C. Zhang, Y. Liu, X. Nan and G. Cao, *J. Phys. Chem. C*, 2015, **119**, 11391.
- G. Zhou, F. Li and H. Cheng, *Energy Environ. Sci.*, 2014, **7**, 1307.
- Y. Tang, Y. Zhang, J. Deng, D. Qi, W. R. Leow, J. Wei, S. Yin, Z. Dong, R. Yazami, Z. Chen and X. Chen, *Angew. Chem., Int. Ed.*, 2014, **126**, 13706.
- L. Hu, J. W. Choi, Y. Yang, S. Jeong, F. La Mantia, L. F. Cui and Y. Cui, *Proc. Natl. Acad. Sci. U. S. A.*, 2009, **106**, 21490.
- L.-F. Cui, L. Hu, J. W. Choi and Y. Cui, *ACS Nano*, 2010, **4**, 3671.
- S. Y. Chew, S. H. Ng, J. Wang, P. Novak, F. Krumeich, S. L. Chou, J. Chen and H. K. Liu, *Carbon*, 2009, **47**, 2976.
- L. F. Cui, L. Hu, J. W. Choi and Y. Cui, *ACS Nano*, 2010, **4**, 3671.
- M. Ghidui, M. R. Lukatskaya, M.-Q. Zhao, Y. Gogotsi and M. W. Barsoum, *Nature*, 2014, **516**, 78.
- L. Zhang, W. Fan and T. Liu, *RSC Adv.*, 2015, **5**, 54.
- L. Hu, D. S. Hecht and G. George, *Chem. Rev.*, 2010, **110**, 5790.
- Z. Chen, V. Augustyn, X. Jia, Q. Xiao, B. Dunn and Y. Lu, *ACS Nano*, 2012, **6**, 4319.
- I. Mjejri, N. Etteyeb and F. Sediri, *J. Alloys Compd.*, 2014, **611**, 372.
- C. Tang, J. Sheng, C. Xu, S. N. B. Khajebashi, X. Wang, P. Hu, X. Wei, L. Zhou and L. Mai, *J. Mater. Chem. A*, 2015, **3**, 19427.
- K. Zhao, F. Liu, C. Niu, W. Xu, Y. Dong, L. Zhang, S. Xie, M. Yan, Q. Wei, D. Zhao and L. Mai, *Adv. Sci.*, 2015, **2**, 1500154.
- T. Brezesinski, J. Wang, J. Polleux, B. Dunn and S. H. Tolbert, *J. Am. Chem. Soc.*, 2009, **131**, 1802.
- Q. Wei, Z. Jiang, S. Tan, Q. Li, L. Huang, M. Yan, L. Zhou, Q. An and L. Mai, *ACS Appl. Mater. Interfaces*, 2015, **7**, 18211.